



The centrifugal acceleration and the Y-point of the Pulsar Magnetosphere

SHINPEI SHIBATA ¹ AND SHOTA KISAKA ²

¹ Faculty of Science, Yamagata University

Kojirakawa 1-4-12, Yamagata 990-8560, JAPAN

² Physics Program, Graduate School of Advanced Science and Engineering, Hiroshima University,
Higashi-Hiroshima 739-8526, Japan

ABSTRACT

We investigate the centrifugal acceleration in an axisymmetric pulsar magnetosphere under the ideal-MHD approximation. We solved the field-aligned equations of motion for flows inside the current sheet with finite thickness. We find that flows coming into the vicinity of a Y-point become super fast. The centrifugal acceleration takes place efficiently, and most of the Poynting energy is converted into kinetic energy. However, the super fast flow does not provide enough centrifugal drift current to open the magnetic field. Opening of the magnetic field is possible by the plasmas that are accelerated in the azimuthal direction with a large Lorentz factor in the closed field region. We find that this acceleration takes place if the field strength increases toward the Y-point from inside. The accelerated plasma is transferred from the closed field region to the open field region by magnetic reconnection with plasmoid emission. We also estimate the Lorentz factor to be reached in the centrifugal wind.

Keywords: Rotation powered pulsars (1408) — High energy astrophysics (739) — Magnetohydrodynamics (1964) — Plasma astrophysics (1261)

1. INTRODUCTION

Particle acceleration by pulsars is a long-standing issue in astrophysics. In an early stage of investigation, the idea of the relativistic centrifugal wind is intensively studied (Michel 1969; Goldreich & Julian 1970; Li & Melrose 1994). Since the centrifugal acceleration is based on a corotational motion of the magnetospheric plasmas, plasma density is assumed to be high, and the ideal-MHD condition holds everywhere. In reality, however, acceleration mechanism depends on plasma density, and more specifically on where and how much electron-positron pairs are created. Then particle acceleration by field-aligned electric field also interests us to explain the pulsed emission from radio to gamma-ray (Jackson 1976; Cheng et al. 1976; Takata et al. 2011; Ruderman & Sutherland 1975; Shibata 1997; Timokhin 2010). Recently, Particle-in-Cell (PIC) simulations are applied to understand the global structure of the pulsar magnetosphere (Chen & Beloborodov 2014; Belyaev 2015; Hakobyan et al. 2023; Bransgrove et al. 2023; Hu & Beloborodov 2022). They are able to treat both the field-aligned particle acceleration and the centrifugal acceleration. However, the mechanism of the centrifugal acceleration still remains unresolved. In this paper, we

revisit this problem, and compare with recent PIC simulations.

The model we consider is an axisymmetric steady magnetosphere with a magnetic dipole moment at the center parallel to the angular velocity. The plasma number density is assumed to be much higher than the Goldreich-Julian density everywhere, so that the ideal-MHD approximation holds. We do not deal with pair creation processes.

The magnetospheric plasma tends to corotate with the star. Strict corotation would lead us to a divergence of the Lorentz factor at the light cylinder, i.e.,

$$v_\varphi = \varpi \Omega_* \rightarrow c \quad \text{as } \varpi \rightarrow c/\Omega_* \equiv R_L, \quad (1)$$

where Ω_* is the angular velocity of the star, ϖ is the axial distance, and R_L is the radius of the light cylinder. In reality, just within the light cylinder, the inertia would be so large that the centrifugal drift current would open the magnetic field lines. The plasma accelerated in azimuthal direction with a large Lorentz factor would finally be thrown away along the open field lines. This is the idea of the centrifugal acceleration, just like a trebuchet.

However, after some works (eg., Michel 1969; Begelman & Li 1994; Takahashi & Shibata 1998), it is con-

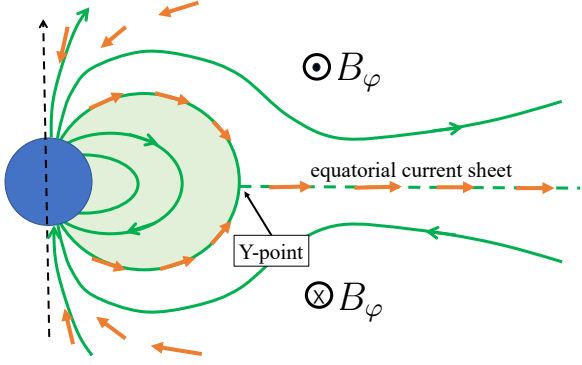


Figure 1. Schematic picture of an axisymmetric magnetosphere with close and open magnetic field lines. The small arrows indicate poloidal currents, which form a loop in each hemisphere starting from the star in lower latitudes and go back to the star in higher latitudes. The top of the close field lines is a junction of the current sheets in the force-free limit, called a Y-point.

cluded that the centrifugal acceleration is inefficient, and flows on the open field lines are Poynting energy dominant. There is toroidal magnetic field B_φ due to the global current loop as shown in Figure 1. The azimuthal velocity does not follow the corotation but does the isorotation law, $v_\varphi = \Omega_* \varpi + \kappa B_\varphi$, where κ is a scalar function to be determined. The open magnetic field lines trail backward due to rotation, resulting in negative κB_φ , meaning departure from the corotation. Thus the slingshot acceleration fails. A typical Lorentz factor to be reached is $\sigma_*^{1/3}$ (Michel 1969, and elsewhere) where $\sigma_* = B^2/4\pi nmc^2$, is the magnetization parameter, and B and n are the field strength and the number density, respectively. An expression $\sigma_* = \gamma_{\max}/2\mathcal{M}$ may be useful, where $\gamma_{\max} = eB_L/mc\Omega_*$ is the maximum reachable Lorentz factor, $\mathcal{M} = n/(\Omega_* B_L/2\pi ec)$ is the multiplicity of the plasma, and B_L is the light cylinder field. The value of σ_* gives a typical Lorentz factor when most of the Poynting energy is converted into plasma. A flow with the Lorentz factor of $\sigma_*^{1/3}$ is obviously Poynting energy dominant.

The poloidal current loop has an essential role to carry Poynting energy away from the neutron star, since it generates B_φ and the Poynting flux, $c\mathbf{E}_\perp \times \mathbf{B}_\varphi/4\pi$, where \mathbf{E}_\perp is the electric field across the magnetic field produced by the electromotive force of the star. Due to symmetry, however, the equatorial plane is the place where the toroidal field vanishes. In a region where the toroidal field becomes very weak, the plasma motion may become very close to the pure corotation to get large Lorentz factors. Such a place is where the equatorial current sheet touches the closed field region, a vicinity of a so-called Y-point (Figure 1).

Meanwhile, highly accurate PIC simulations are available to provide detailed analysis for the centrifugal acceleration (Chen & Beloborodov 2014; Belyaev 2015; Hakobyan et al. 2023; Bransgrove et al. 2023; Hu & Beloborodov 2022). It has been shown that most of the space outside the equatorial current sheet is Poynting energy dominant. However, Poynting energy is converted to kinetic energy in the vicinity of the Y-point and the equatorial current sheet. It is interesting that Hu & Beloborodov (2022) show an acceleration in azimuthal direction such as expected in the centrifugal acceleration. Another interesting feature of their simulations is ejection of plasmoids.

In this paper, we study the centrifugal acceleration that is expected in a vicinity of the Y-point. It will be shown that super-fast flows appear inside the thin current layer. The centrifugal drift current opens the poloidal magnetic fields in the vicinity of the Y-point. We will propose a self-consistent structure of the centrifugal wind.

2. MAGNETIC FIELD OPENING BY THE CENTRIFUGAL DRIFT CURRENT

Let us estimate the Lorentz factor to open the magnetic field lines by centrifugal drift currents. The region we consider is a vicinity of the Y-point. In the following sections, we use the cylindrical coordinate (z, ϖ, φ) with the unit vectors denoted by $(\mathbf{e}_z, \mathbf{e}_\varpi, \mathbf{e}_\varphi)$. The centrifugal drift velocity, which has opposite directions depending on the charge sign, would be

$$\mathbf{v}_d = c \frac{\mathbf{F} \times \mathbf{B}}{\pm eB^2} \approx \pm \frac{\gamma mc^2}{eB_Y R_Y} c \mathbf{e}_\varphi, \quad (2)$$

where the centrifugal force on an electron of mass m and the Lorentz factor γ is evaluated as $\mathbf{F} = (\gamma mc^2/R_Y)\mathbf{e}_\varpi$, $R_Y \sim R_L$ is the axial distance of this region, and B_Y is the magnetic field that is weakened significantly as compared with B_L . The drift current density may be $j_\varphi = 2en|\mathbf{v}_d| \approx 2nc(\gamma mc^2/B_Y R_Y)$. Applying Ampère's law for a closed loop in the $\varpi - z$ plane around the Y-point, we have $(4\pi/c)j_\varphi \Delta = 2B_p^{(\text{out})}$ for a condition of opening the magnetic field, where $B_p^{(\text{out})} \approx B_L$ is the poloidal field strength outside the current layer, and Δ is a typical thickness. With these conditions, we have the Lorentz factor to open the magnetic field,

$$\gamma_c \approx \frac{(B_p^{(\text{out})})^2}{4\pi nmc^2} \frac{R_Y}{\Delta} \frac{B_Y}{B_p^{(\text{out})}} = \sigma_* \frac{R_Y}{\Delta} \frac{B_Y}{B_p^{(\text{out})}}. \quad (3)$$

We expect a thin layer, $\Delta \ll R_Y$, and weak magnetic field, $B_Y \ll B_L$. If $(R_Y/\Delta)(B_Y/B_L) \approx 1$, $\gamma_c \approx \sigma_*$. It is one of our objectives to find Δ and B_Y in a self-consistent manner, considering the magnetohydrodynamics inside the current layer.

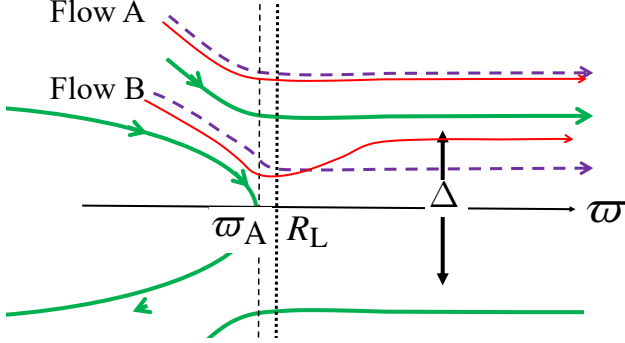


Figure 2. Two types of field-aligned flows. Flow A and Flow B, respectively, runs outside and inside the current layer with the thickness Δ . The dashed curves are their stream lines. The solid curves are the magnetic field lines. The thin red curves are the poloidal current lines. The ϖ -axis indicates the axial distance. The thin dashed line $\varpi = \varpi_A$ is the Alfvén surface. The thin dotted line $\varpi = R_L$ is the light cylinder.

3. CURRENT DISTRIBUTION IN THE CURRENT SHEET

In the following calculations of field-aligned flows, we assume an axisymmetric magnetosphere with the ideal-MHD condition.

Let us consider two flows: one runs just outside the equatorial current layer, the other runs inside. We call them Flow A and Flow B, respectively, as shown in Figure 2. What is distinctive of Flow B from Flow A is significant decrease in the poloidal field strength as is flows near the Y-point. We expect that the centrifugal acceleration is inefficient in Flow A, but efficient in Flow B.

Flows such as Flow A and Flow B can be solved by using the field-aligned equations (Okamoto 1978; Camenzind 1986; Takahashi 1991), provided that a poloidal field is given. It must be noticed here that the solution of field-aligned flows determines values of B_φ and in turn the current function $I = \varpi B_\varphi$, where stream lines of the poloidal current is given by contours of I . The field-aligned equations are solved with a given set of boundary conditions and the condition that the solution passes through the fast critical point. As a result, I is uniquely determined. On the other hand, as was done in obtaining the force-free solution (Contopoulos et al. 1999; Timokhin 2006), the trans-field equation that gives the poloidal field structure determines the current function I so that the field lines are regular on the Alfvén surface, which coincides with the light cylinder in the force-free limit. Thus, the both systems of equations can determine I . The pulsar problem is only solved simultaneously the field-aligned equations and the trans-

field equation, i.e., the two I 's obtained in the two ways must be identical. This has never been done so far.

The force-free solution may be a good approximation for the field structure in high and middle latitudes, because the field-aligned solutions give weak centrifugal acceleration there. This is supported by the PIC simulations and the Relativistic Magnetohydrodynamic simulations, which give the results very similar to the force-free solution.

The problem is how the current runs inside the current layer and in the vicinity of the Y-point.

For flows such as Flow A, the poloidal current lines almost coincide with the flow stream lines, since the centrifugal acceleration is weak. If a strong acceleration takes place on Flow B, the current stream lines crosses the flow stream line causing the acceleration. In this case, some current lines converge to the Y-point as indicated in Figure 2, forming a very thin current sheet. This seems a realization of the infinitely thin current sheet that is required by the regularity on the light cylinder in the force-free approximation. Even if inertia is taken into account in the trans-field equation, the inertial effect may not be significant on the Alfvén surface; the acceleration become significant beyond the Alfvén surface. Therefore, the thin current sheet on the Alfvén surface would be a genuine property of the centrifugal wind, ensuring the regularity of the poloidal magnetic field.

4. FIELD-ALIGNED FLOWS IN THE CURRENT LAYER

In this section, we solve the field-aligned equations for Flow A and B. The field-aligned equations are composed of the three conservation laws and the iso-rotation law. Given a stream function ψ of the poloidal magnetic field, the particle flux $g(\psi)$, the angular momentum $\ell(\psi)$, and the energy $\epsilon(\psi)$ are functions of ψ only. In the iso-rotation law, the angular velocity $\Omega(\psi)$ is also a function of ψ . These quantities are all determined by a set of boundary conditions and the condition that the flow passes through a fast-critical point.

The field-aligned equations are algebraic equations, and are joined into a single expression called the Bernoulli function $\epsilon(\xi, v)$. Here, we normalize the axial distance ϖ and the poloidal 4-velocity u_p by the values at the Alfvén point, i.e., $\xi = \varpi/\varpi_A$ and $v = u_p/u_A$.

The field-aligned equations are algebraic equations, and are joined into a single expression called the Bernoulli function $\epsilon(\xi, v)$. Here, we normalize the axial distance ϖ and the poloidal 4-velocity u_p by the values at the Alfvén point, i.e., $\xi = \varpi/\varpi_A$ and $v = u_p/u_A$. A non-dimensional form of the Bernoulli function $\epsilon(\xi, v)$

with the definition of the Alfvén point (Okamoto 1978; Camenzind 1986; Takahashi 1991) is given below, and it is notable that a solution is obtained as a curve $\epsilon(\xi, v) = \text{constant}$ on the ξ - v plane. The Bernoulli function $\epsilon(\xi, v)$ has two non-dimensional parameters,

$$\lambda = \frac{\Omega(\psi)\ell(\psi)}{\epsilon(\psi)}, \quad (4)$$

and

$$\sigma = \frac{\Omega(\psi)^2 B_p \varpi^2}{4\pi m c^3 g(\psi)}, \quad (5)$$

and it has a singularity at the Alfvén point, $\varpi_A = \sqrt{\lambda} c / \Omega(\psi)$. The 4-velocity at the Alfvén point becomes $u_A = (1 - \lambda)\sigma_A / \lambda$, where σ_A is the value of σ at the Alfvén point. The Bernoulli function has a form

$$\left(\frac{\epsilon(\xi, v)}{m c^2} \right)^2 = \frac{(1 + u_p^2)}{(1 - \lambda)^2} \frac{[1 - \lambda \xi^2 - (1 - \lambda)v \xi^2]^2}{(1 - v \xi^2)^2 - \lambda \xi^2 (1 - v)^2}, \quad (6)$$

where

$$u_p = \frac{1 - \lambda}{\lambda} \sigma v. \quad (7)$$

A family of solutions is easily drawn as contours of $\epsilon(\xi, v)$ for a given set of λ and σ .

We chose one solution among them that passes through the fast-critical point; hereafter we denote the fast point as (ξ_f, v_f) . At the same time, the flow energy $\epsilon_f = \epsilon(\xi_f, v_f)$ is obtained as if it is an eigenvalue.

The Bernoulli function $\epsilon(\xi, v)$ has the two parameters, λ and σ . However, the value of λ is determined implicitly by given inner boundary conditions. Firstly we assume λ , and obtain a critical solution. Then we examine whether the solution satisfies the set of given boundary conditions. If not, we change λ until the boundary conditions are satisfied. The inner boundary conditions are those for a plasma source region. More specifically, for Flow A and Flow B, they may be such that the plasma is injected well within the light cylinder $\xi \ll 1$ with the Lorentz factor $\gamma \sim 1$.

Thus, σ is the only parameter that determines the flow. It is decomposed into two factors:

$$\sigma = \sigma_0 \hat{B}, \quad (8)$$

$$\sigma_0 = \frac{B_L}{4\pi m c g(\psi)} = \gamma_{\max} \left(\frac{v_p/c}{\mathcal{M}} \right)_{\text{in}} \left(\frac{\Omega_*}{\Omega(\psi)} \right) \approx \frac{\gamma_{\max}}{\mathcal{M}_{\text{in}}} \quad (9)$$

$$\hat{B} = \frac{B_p \varpi^2}{B_L R_L^2}, \quad (10)$$

where $g(\psi) = n\kappa = n v_p / B_p$, and \mathcal{M}_{in} is the parameter of the plasma number density at the inner boundary, i.e., $\mathcal{M}_{\text{in}} = n / [\Omega(\psi) B_p / 2\pi c e]$, evaluated at the inner boundary. The configuration of the poloidal magnetic field only comes into the parameter $\hat{B} \propto B_p \varpi^2$.

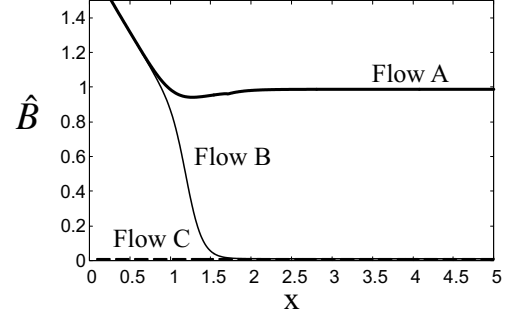


Figure 3. Models of $\hat{B}(x) \propto B_p \varpi^2$ for Flow A, Flow B and Flow C.

The key parameter that makes difference between Flow A and Flow B is \hat{B} . The poloidal magnetic field would be something like dipole near the star, and changes to something like radial near and beyond the light cylinder. Mimicking this, a simple function for \hat{B} is introduced as follows. The magnetic stream function for a dipole field is $\psi = B_L R_L^3 \varpi / r^2$, where $r = (z^2 + \varpi^2)^{1/2}$. For the dipole field, \hat{B} is given by

$$\hat{B}_{\text{dip}}(x) = (\psi / B_L R_L^2) \left[4 - 3(\psi x / B_L R_L^2)^{2/3} \right]^{1/2}, \quad (11)$$

where $x = \varpi / R_L$. Since \hat{B} is constant for a radial field, we assume that it gradually changes to a constant, $\hat{B}_{\text{radial}} = \hat{B}_{\text{dip}}(x_c)$ beyond a certain point x_c . Then we assume that \hat{B} for Flow A is

$$\hat{B}_a(x) = S \left(\frac{x_c - x}{\delta_c} \right) \hat{B}_{\text{dip}}(x) + S \left(\frac{x - x_c}{\delta_c} \right) \hat{B}_{\text{radial}}, \quad (12)$$

where $S(x) = 1 / [\exp(-x) + 1]$ is the sigmoid function (see Figure 3).

As an example of Flow A, we take $\gamma_{\max} = 10^7$ and $\mathcal{M}_{\text{in}} = 10^3$, and therefore $\sigma_0 = 10^4$. The solutions in the ξ - v plane are shown in Figure 4, where the critical solution is colored in red. It is known that all the solutions pass through the Alfvén point. The denominator of (6) must be positive, so that there is a forbidden region, which is bounded by the two curves,

$$v_+ = \frac{1 + \sqrt{\lambda} \xi}{\xi(\xi + \sqrt{\lambda})}, \quad v_- = \frac{1 - \sqrt{\lambda} \xi}{\xi(\xi - \sqrt{\lambda})}, \quad (13)$$

indicated by the dashed curves in the figure. The critical points are the points where the two curves, $\partial \epsilon / \partial v = 0$ and $\partial \epsilon / \partial \xi = 0$ meet. These curves are also shown with the dots in Figure 4. Since \hat{B} is essentially constant beyond the Alfvén point, the X-type critical point, namely the fast point, goes to infinity as in the case of the radial flow. After an iteration, the value of λ is determined so

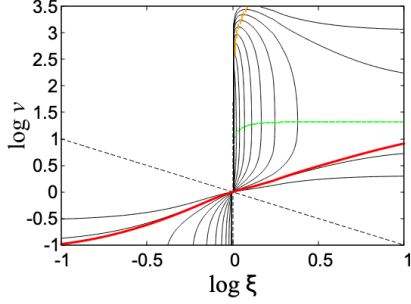


Figure 4. A family of the solutions and the critical solution (red) of Flow A. The dashed curves indicate the boundaries of the forbidden region. The green and orange dots indicate where $\partial\epsilon/\partial v = 0$ and $\partial\epsilon/\partial\xi = 0$, respectively.

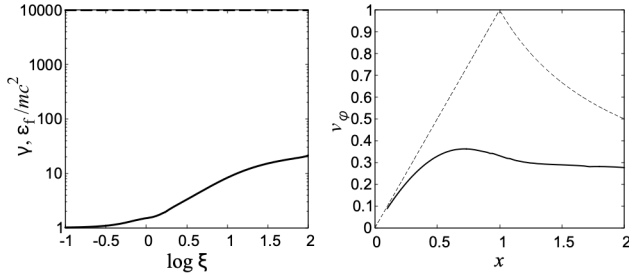


Figure 5. Properties of Flow A. Left panel: The particle energy γ (solid curve), and the total energy ϵ_f (dashed line) as functions of $\log \xi$. Right panel: The azimuthal velocity v_ϕ as a function of $x = r/R_L$. The dashed curve indicates the corotation for $x < 1$ and the free emission tangent to the light cylinder for $x > 1$.

that the injection point locates at about $\xi = 0.1$. The obtained parameters of the critical solution is given in Table 1.

The critical solution gives $\gamma = 21.4$ at $\xi = 100$, which is consistent with the Michel's solution $\gamma \rightarrow \epsilon_f^{1/3} = 21.5$ as $\xi \rightarrow \infty$ for the radial flow. The total energy ϵ_f is $\approx \sigma_0$. In the left panel of Figure 5, we plot γ as a function of $\log \xi$ with ϵ_f/mc^2 , which is constant. Flow A is a Poynting dominant flow. The azimuthal velocity deviates from the corotation as seen in the right panel of Figure 5.

Next, we consider Flow B that comes into a weak field region near the Y-point. We expect a significant decrease of \hat{B} beyond the Alfvén point. We model \hat{B} by

$$\hat{B}_b(x) = \left[(1 - D) S \left(\frac{x_d - x}{\delta_d} \right) + D \right] \hat{B}_a, \quad (14)$$

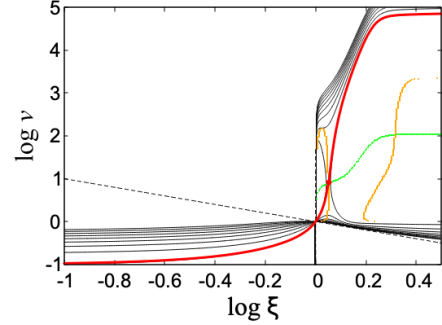


Figure 6. The same as Figure 4, but for the flow B.

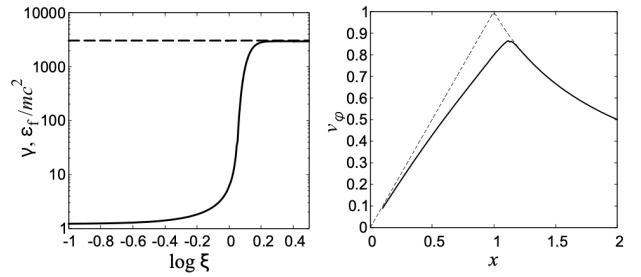


Figure 7. The same as Figure 5, but for Flow B.

where D and x_d , respectively, determine how much and where the magnetic field decreases. If $D = 1$, there is no decrease, but if $D < 1$, \hat{B} drops down to $D\hat{B}_a$ beyond x_d . In the following example, we use $D = 0.01$, $x_d = 1.2$, and $\delta_d = 0.1$, as shown in Figure 3. The value of σ_0 is the same as Flow A, i.e., $\sigma_0 = 10^4$.

There is a topological change in the solution curves as shown in Figure 6. An X-type critical point, the fast point, appears just beyond the Alfvén point; $\xi_f = 1.13$. The Lorentz factor grows up around the fast point from the value at the injection ($\gamma = 1.1$) to 2.95×10^3 , which corresponds to 98% of the total energy ϵ_f (Figure 7). In contrast with Flow A, deviation of the azimuthal velocity from the corotation is weaker, and v_ϕ peaks at $\sim 0.85c$. More importantly the curve eventually almost follows the analytic curve of the tangential ejection with the light speed at the Alfvén radius. The flow is effectively corotation up to the Alfvén point. The total energy ϵ is about 30% of Flow A. This is reasonable because the energy flux of Flow B is on its way of decreasing down to zero on the equator.

It is known that a decrease of \hat{B} causes efficient conversion from the Poynting energy to kinetic energy in

Table 1. Some parameters for the critical solution.

Type	σ_0	$\log \xi_f$	$\log v_f$	ϵ_f	$1 - \lambda$	$1 - x_A$	γ
Flow A	10^4	∞	1.3275	0.9905×10^4	1.02×10^{-4}	5.15×10^{-5}	21.4(a)
Flow B	10^4	0.0525	0.9075	3.039×10^3	4.0×10^{-4}	2.0×10^{-4}	2.95×10^3 (b)
Flow C (c)	10^4	1	1	10^2	4.0×10^{-4}	2.0×10^{-4}	10^2

(a): evaluated at $\xi = 100$, (b): evaluated at $\xi = 3.14$, (c): λ is assumed.

the context of the AGN jets that have a collimated geometry (Camenzind 1989; Begelman & Li 1994).

5. CENTRIFUGAL DRIFT CURRENT OF FLOW B

Our next question is whether the super fast flow such as Flow B can provide enough centrifugal drift current to open magnetic field lines. We take the same way as we derive (3), but we use $v_d = \pm(c/e)(\gamma m v_\varphi^2 / R_Y B_Y)$ and $n v_p / B_p = g(\psi)$ to evaluate the density. Then we have

$$\frac{\Delta}{R_Y} = \frac{(v_p/c)}{(v_\varphi/c)^2} \frac{\sigma_0}{\gamma} \frac{B_Y}{B_p} \frac{B_p^{(\text{out})}}{B_L}. \quad (15)$$

If the drift current is enough large, then Δ/R_Y must be much smaller than unity. However, this expression indicates that Δ/R_Y will never be small. The last factor $B_p^{(\text{out})}/B_L$ is about unity. The factor B_Y/B_p will not be much smaller than unity. The effective field to produce the drift current is z -component of the poloidal field. The region with a large azimuthal velocity would be where the flow comes into the Y-point, and the ratio of the z -component to the poloidal component of the flow will not be so small. Moreover, if the Y-point is actually T-point as suggested by Contopoulos et al. (2024), it becomes unity. The ratio σ_0/γ can be small, if $\gamma \gg \sigma_0$. However, a very efficient acceleration gives at most $\gamma \sim \sigma_0$. Since v_φ is something around ~ 0.85 , the factor $(v_p/c)/(v_\varphi/c)^2$ will not be very small. In conclusion, accelerated flows such as Flow B will not produce enough current to open the magnetic field. This may sound strange when one compares with (3). However, as is seen in the expression $n = g(\psi) B_p / v_p$, the plasma density decreases due to the decrease of the magnetic field or increase of the cross section of the flow. As a result, even if the centrifugal acceleration becomes efficient, the drift current density does not increase.

6. PLASMA INJECTION AT THE Y-POINT

The reason why sufficient drift current to open magnetic field lines cannot be obtained is due to decrease in flow density as the flow comes into the weak field region around the Y-point. The magnetic field should be opened in the centrifugal wind. One possible and very likely way to avoid the density decrease is an injection of plasma at the Y-point. Let us consider a flow injected

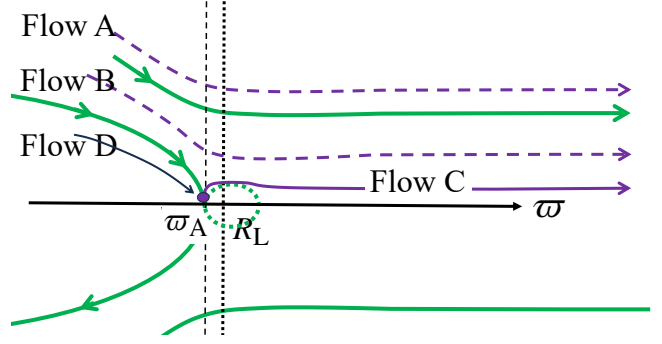


Figure 8. Flow C injected just within the Alfvén point, and Flow D is a flow before the injection.

from a top of the closed field region into the current layer, such as Flow C in Figure 8.

The parameters characterize Flow C would be such that \hat{B} stays small throughout from injection (Figure 3), and that σ_0 is also small. In the definition (9) of σ_0 , the density parameter \mathcal{M}_{in} is calculated at the injection point where the magnetic field is weak around the Y-point. Therefore, \mathcal{M}_{in} is much larger than a multiplicity based on a typical Goldreich-Julian density, $\Omega_* B_L / 2\pi c e$.

For an example of Flow C, we suppose that the magnetic field strength at the injection point is one hundredth of the field outside the current layer. Then, $\sigma_0 = 10^4$ of Flow A and B is reduced to $\sigma_0 = 100$ for Flow C, and $\hat{B} = \hat{B}_c = \text{constant} = 0.01$ for Flow C.

A family of the solutions is shown in Figure 9. We find another topology for Flow C. Although \hat{B} is constant, the topology is different from the Michel's radial-field solution. The two curves $\partial\epsilon/\partial\xi = 0$ and $\partial\epsilon/\partial v = 0$ meet at large distance, where an O-type critical point appears. On the other hand, the X-type critical point seems to go to the Alfvén point as shown in a closeup view (the right panel of Figure 9). The numerical solutions suggest that both $\partial\epsilon/\partial v = 0$ and $\partial\epsilon/\partial\xi = 0$ curves approach the Alfvén point tangentially to the v -axis. Thus, the critical solution becomes the vertical line coinciding with the v -axis as far as v is not so large. Other solutions are two-valued functions of ξ , and are inappropriate. When $\xi = 1$ with $v \neq 1$, the Bernoulli function becomes

$$\left(\frac{\epsilon(1, v)}{mc^2} \right)^2 = \frac{1}{1 - \lambda} \left[1 - \left(\frac{1 - \lambda}{\lambda} \right)^2 \sigma^2 v^2 \right]. \quad (16)$$

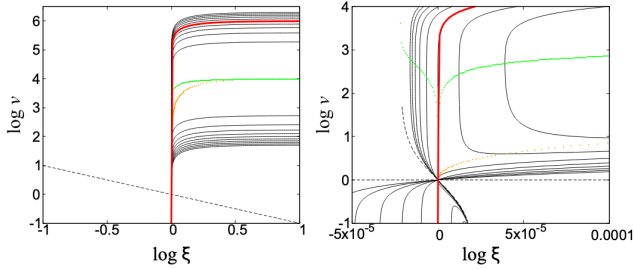


Figure 9. Left panel: The critical solution for Flow C injected just inside of the Alfvén point. Right panel: A close-up view around the Alfvén point.

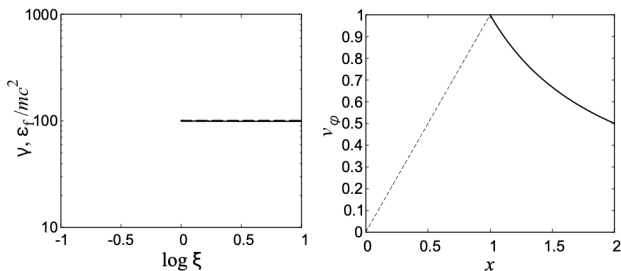


Figure 10. Properties of Flow C. Left panel: The Lorentz factor (solid line) and the energy of the flow (dashed line) as functions of $\log \xi$. Right panel: The azimuthal velocity as a function of x .

It follows from this expression that in the limit $1 - \lambda \rightarrow 0$, in other words, the centrifugal-driven limit, the fast energy is $\epsilon_f = (1 - \lambda)^{-1/2}$, regardless of σ . Figure 10 is drawn for $1 - \lambda = 10^{-4}$, and therefore $\epsilon_f = 100$. In this case, the injection point is always very closed to the Alfvén point, as we intend. The topology of this type is not new but has been studied by [Takahashi \(1991\)](#), and applied in the context of a disc wind around compact stars.

The Lorentz factor of the flow and the azimuthal velocity are shown in Figure 10. It can be seen that the flow energy is injected totally as kinetic energy. Since $\lambda = \Omega \ell / \epsilon \approx 1$, angular momentum is brought in as well.

In contrast with Flow A and Flow B, we cannot determine the value of λ and therefore $\gamma = (1 - \lambda)^{-1/2}$ since the critical solutions are degenerated. Determination of λ is postponed until a self-consistent treatment of plasma injection and determination of the poloidal field.

Pair creation in the vicinity of the Y-point is one of the injection process, but a most efficient way would be mag-

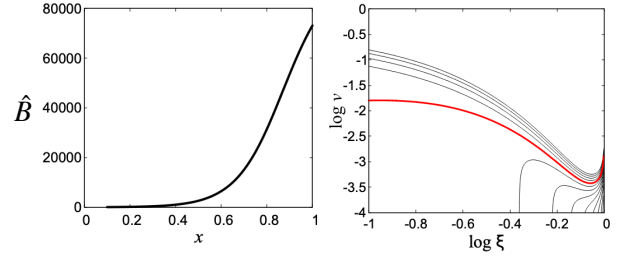


Figure 11. \hat{B} (left) and the family of the solutions (right) of Flow D.

netic reconnection. At the top of the closed field region, a high density corotating plasma with a large Lorentz factor accumulates, and is likely to be transferred to the open field region via magnetic reconnection. In this case the value of σ_0 / γ in (15) would be very small, meaning that the toroidal current is enough strong to open the magnetic field, where note again that the face value of σ_0 is reduced in Flow C. The reconnection process will be associated with plasmoid emission (the dashed small loop in Figure 8). The injection may be intermittent. We suppose that the plasmoid formation seen in PIC simulations corresponds to this injection process.

Since the MHD equation of motion in the cold limit is equivalent to the equation of motion of individual particles, it is likely that the motion of plasmoids follows the solution of Flow C.

7. PRE-ACCELERATION IN THE CLOSED FIELD REGION

Before the injection, the plasma that resides in the closed field region must be accelerated in the azimuthal direction. In a steady state, such plasmas migrate from the inner magnetosphere to the top of the closed region. This type of flow can also be described by the field-aligned equation. Let us call this Flow D. We again assume $\sigma_0 = 10^4$, and look for a solution with the expected properties. The only parameter we can change is \hat{B} . We find that the expected flow appears if \hat{B} increases as $\xi \rightarrow 1$. It is known in the force-free model that the poloidal field strength diverges as the Y-point is approached to the light cylinder ([Lyubarskii 1990](#); [Uzdensky 2003](#); [Timokhin 2006](#)). This increase of magnetic field plays a key role in Flow D.

To give an illustrative solution for Flow D, we use the same model (14) for \hat{B} , but we take a set of parameters, $D = 10^5$, $x_d = 0.9$, and $\delta_d = 0.1$, mimicking a quick increase of \hat{B} just before the Alfvén point. We denote this model by $\hat{B}_d(x)$ as shown in Figure 11. The right

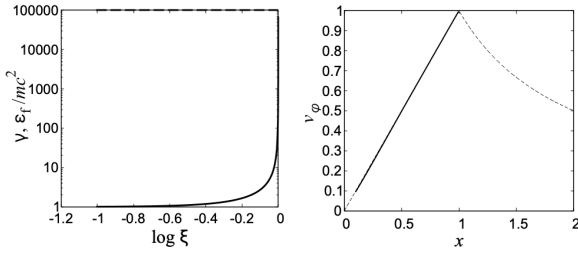


Figure 12. The Lorentz factor (solid line) and the energy of the flow (dashed line) as functions of $\log \xi$, and the azimuthal velocity as a function of x for Flow D.

panel shows the family of the solutions for $\sigma_0 = 10^4$ and $1 - \lambda = 10^{-5}$. The value of λ is chosen so that $\gamma = 1$ at injection. As shown in Figure 12, the Lorentz factor grows up to $\approx \hat{B}_d(x_A) \approx 10^5$ as $\xi \rightarrow 1$, and the azimuthal velocity follows the corotation. Since $\sigma_0/\gamma \ll 1$, the toroidal current is large enough to open the magnetic field.

After some numerical works, we find that $\epsilon \approx \hat{B}_d(x_A)$, $1 - \lambda \approx \epsilon^{-1}$, and $\gamma \rightarrow \hat{B}_d(x_A)$, provided that the injection point is well within the light cylinder, the Lorentz factor is ≈ 1 there, and the azimuthal velocity follows the corotation throughout the flow.

Although the increase of the poloidal field strength in the force-free model is due to the imposed condition of the closed-to-open-field structure via an electromagnetic force balance, we find that this increase is related to increase of inertia and in turn the centrifugal drift current to open the magnetic field. Therefore, a self-consistent treatment of the field-aligned equation and the trans-field equation is expected to give the terminal Lorentz factor and the saturated field strength at the top of the closed field region. Furthermore, the transition from Flow D and Flow C would take place, and therefore magnetic reconnection must be included in the self-consistent treatment.

8. DISCUSSION

Our results seem aligned well with the recent results of PIC simulations (Chen & Beloborodov 2014; Belyaev 2015; Hakobyan et al. 2023; Bransgrove et al. 2023; Hu & Beloborodov 2022), in which kinetic energy dominant flows appear around the equatorial current sheet, and plasmoids are ejected from the top of the last closed field lines. More importantly, Hu & Beloborodov (2022) showed that plasmas are accelerated in the azimuthal direction with high Lorentz factors near the top of the closed field region, and that the plasmas are re-

leased away freely by reconnection and plasmoid emission. These two steps correspond to Flow D and Flow C, respectively. Comparison between their results and our results would be a future issue.

A problem found in the previous sections is that our model does not predict the thickness of the current sheet or the Lorentz factor to be reached. This is because the fast critical point degenerates into the Alfvén point under the circumstances of equipartition between the magnetic field and the plasma energy densities ($\sigma \sim 1$). We need to undertake reconnection processes. However, before that, we can make an estimate by assuming that the thickness is of order of Larmor radius (Asano et al. 2004; Hoshino 2020). We employ (3), where we set $B_p^{(\text{out})} \approx B_L$, and the density is the value in the Y-point, denoted by n_Y , which is distinguished from the density outside the current sheet, n . With the condition $\Delta \sim (eB/\gamma mc^2)^{-1}$, where we assume $B \approx B_L$ as a mean value of a strong field in the closed region and a weak field in the open region, (3) yields

$$1 \approx \frac{2\mathcal{M}\gamma^2(mc^2)^2}{(eB_L R_L)^2} \frac{B_L}{B_Y} \frac{n_Y}{n}. \quad (17)$$

The continuity implies $(B_L/B_Y)(n_Y/n) \approx 1$ for the both sides of the Y-point. Then we have

$$\gamma \approx \frac{\gamma_{\max}}{(2\mathcal{M})^{1/2}}, \text{ and } \frac{\Delta}{R_L} \approx \frac{1}{(2\mathcal{M})^{1/2}}. \quad (18)$$

We also find that the drift velocity is well below c by a factor of $1/(2\mathcal{M})^{1/2}$. We suggest that the highest energy can be much higher than a simple estimate of $\gamma_{\max}/\mathcal{M}$. We may hopefully verify the efficiency factor $\mathcal{M}^{-1/2}$ by the future PIC simulations.

A significant difference between the present model and the previous PIC simulations is the location of the Y-point. In our previous particle simulations (see Figure 5 of Yuki & Shibata (2012)), we have implied that field-aligned potential drop inside the light cylinder makes a superrotation, and the Y-point move inward. The PIC simulation by Hu & Beloborodov (2022) also shows supercorotation. In their simulation, there is field-aligned acceleration around the null surface. The field-aligned acceleration, superrotation, and subrotation are interact to each other to establish the proper net loss of the angular momentum as shown in Shibata & Kisaka (2021).

Another possible reason for the Y-point within the light cylinder is that λ becomes much smaller than unity. This case can happen if the plasma injected into the magnetosphere has high density and bring a large amount of energy. The introduced kinetic and thermal energy contribute partly to drive wind.

It is certain that the acceleration in the azimuthal direction takes place in the closed field region, so that if \mathcal{M}

is not so large, where Larmor radius becomes comparable with the light radius, then reconnection would start within the light cylinder. This also can be a reason that the Y-point seems to locate inside the light cylinder.

Contopoulos et al. (2024) discussed an increase of the poloidal magnetic field just inside the Y-point. The increase would be caused by the close-open structure imposed by hand in the force-free model. We have found that the increase is essential for the acceleration in the azimuthal acceleration in the sub-Alfvénic flow. Although the electromagnetic force balance with the close-open structure requires the increase of the magnetic field, the increase results in the particle acceleration, and the force balance will be achieved with plasma inertia. In reality, the closed-open structure is maintained by the intermittent plasmoid emission. The system is then sub-steady.

9. CONCLUSIONS

We investigate the centrifugal acceleration in an axisymmetric pulsar magnetosphere under the ideal-MHD approximation. Anticipating the poloidal field structure we have solved the field-aligned equations for different field lines to obtain a hint toward a self-consistent view of the centrifugal wind. The poloidal field structure comes into the flow model through $\hat{B} \propto B_p \varpi^2$.

Flows on the open field lines running apart from the equatorial current sheet, called Flow A, are Poynting energy dominant, and there is no efficient centrifugal acceleration. Flow B that comes into the vicinity of a Y-point and goes out in a current layer with finite thickness is characterized by decrease of \hat{B} just beyond the Alfvén point. Flow B becomes a super fast flow, and the centrifugal acceleration takes place efficiently. However, the centrifugal drift current is not enough to open the magnetic field lines. Flow D is a flow coming from an inner part of the magnetosphere and reaches the top of the closed field region. The key feature of Flow D is an increase of the poloidal field strength toward the Alfvén point, the loop top. The azimuthal velocity follows the corotation, and the plasma gains a very large Lorentz factor, $\gamma \sim \hat{B}(x_A)$. The corotating plasma with a large Lorentz factor produced in Flow D is expected to be injected as Flow C via magnetic reconnection. Flow

C is a super fast flow, and goes out in the equatorial current layer. The region around the junction of the two flows has a centrifugal drift current large enough to open field lines. A jump from Flow D to Flow C requires magnetic reconnection and plasmoid emission.

Although we have not investigated the reconnection process, a simple estimate suggests that the Lorentz factor of the centrifugal driven outflow goes up to

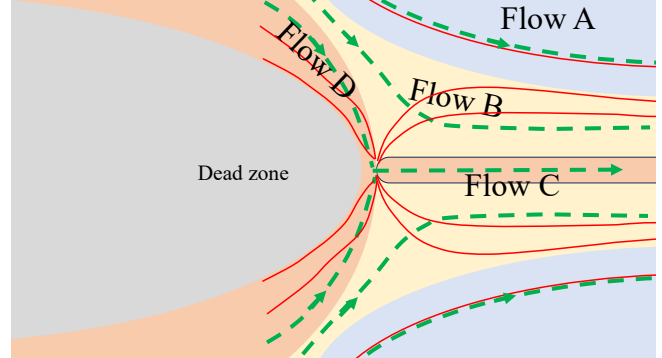


Figure 13. A schematic picture of the vicinity of the Y-point. The locations of Flow A, B, C and D are indicated. The dashed curves are the streamlines, and the thin curves are the poloidal current lines.

$\approx \gamma_{\max} \mathcal{M}^{-1/2}$. In a global point of view, the centrifugal acceleration takes place in a small fraction of $\Delta/R_L \approx \mathcal{M}^{-1/2}$, and the most of the spin-down power is carried by the Poynting energy in the open magnetic flux. The role of the centrifugal force is to open the magnetic field and to establish the poloidal current loop.

The centrifugal acceleration takes place in Flow B and Flow D just outside and inside of the Alfvén point, respectively. The poloidal current lines cross the streamlines there as indicated in Figure 13. As a result, the current sheets shrink at the Y-point. This may be a favored poloidal current distribution if the regularity of the poloidal field on the Alfvén surface requires an infinitely thin current as seen in the force-free solution (Contopoulos et al. 1999; Timokhin 2006).

- 1 This work is supported by KAKENHI 22K03681 (SS,
- 2 SK), 21H01078, and 22H01267 (SK). SS would like to
- 3 thank Professor Masahiro Hoshino for fruitful discus-
- 4 sions on magnetic reconnection.

REFERENCES

- Asano, Y., Mukai, T., Hoshino, M., et al. 2004, *Journal of Geophysical Research (Space Physics)*, 109, A02212.
doi:10.1029/2003JA010114
- Begelman, M. C. & Li, Z.-Y. 1994, *ApJ*, 426, 269.
doi:10.1086/174061
- Belyaev, M. A. 2015, *MNRAS*, 449, 2759

- Bransgrove, A., Beloborodov, A. M., & Levin, Y. 2023, *ApJL*, 958, L9. doi:10.3847/2041-8213/ad0556
- Camenzind, M. 1986, *A&A*, 156, 137
- Camenzind, M. 1989, *Accretion Disks and Magnetic Fields in Astrophysics*, 156, 129. doi:10.1007/978-94-009-2401-7_14
- Cerutti, B., Philippov, A., Parfrey, K., et al. 2015, *MNRAS*, 448, 606. doi:10.1093/mnras/stv042
- Chen, A. Y., & Beloborodov, A. M. 2014, *ApJL*, 795, LL22. doi:10.1088/2041-8205/795/1/L22
- Cheng, A., Ruderman, M., & Sutherland, P. 1976, *ApJ*, 203, 209. doi:10.1086/154068
- Contopoulos, I., Kazanas, D., & Fendt, C. 1999, *ApJ*, 511, 351
- Contopoulos, I., Ntotsikas, D., & Gourgouliatos, K. N. 2024, *MNRAS*, 527, L127. doi:10.1093/mnras/slad153
- Goldreich, P. & Julian, W. H. 1970, *ApJ*, 160, 971. doi:10.1086/150486
- Hakobyan, H., Philippov, A., & Spitkovsky, A. 2023, *ApJ*, 943, 105. doi:10.3847/1538-4357/acab05
- Hoshino, M. 2020, *ApJ*, 900, 66. doi:10.3847/1538-4357/aba59d
- Hu, R. & Beloborodov, A. M. 2022, *ApJ*, 939, 42. doi:10.3847/1538-4357/ac961d
- Jackson, E. A. 1976, *ApJ*, 206, 831. doi:10.1086/154446
- Li, J. & Melrose, D. B. 1994, *MNRAS*, 270, 687. doi:10.1093/mnras/270.3.687
- Lyubarskii, Y. E. 1990, *Soviet Astronomy Letters*, 16, 16
- Michel, F. C. 1969, *ApJ*, 158, 727. doi:10.1086/150233
- Okamoto, I. 1978, *MNRAS*, 185, 69. doi:10.1093/mnras/185.1.69
- Ruderman, M. A. & Sutherland, P. G. 1975, *ApJ*, 196, 51. doi:10.1086/153393
- Shibata, S. & Kisaka, S. 2021, *MNRAS*, 507, 1055. doi:10.1093/mnras/stab2206
- Shibata, S. 1997, *MNRAS*, 287, 262. doi:10.1093/mnras/287.2.262
- Takahashi, M. & Shibata, S. 1998, *PASJ*, 50, 271. doi:10.1093/pasj/50.2.271
- Takahashi, M. 1991, *PASJ*, 43, 569
- Takata, J., Wang, Y., Timokhin, A. N. 2006, *MNRAS*, 368, 1055
- Timokhin, A. N. 2010, *MNRAS*, 408, 2092
- Uzdensky, D. A. 2003, *ApJ*, 598, 446. doi:10.1086/378849
- Yuki, S., & Shibata, S. 2012, *PASJ*, 64, 43